Electronic Supplementary Material (ESI) for Dalton Transactions.

Supporting information for

Synthesis of MOF-based Hg^{2+}-fluorescence probe via stepwise post-synthetic modification in a single-crystal-to-single-crystal fashion and its application in bioimaging

Wen-Yan Li,‡ Song Yang,‡ Yan-An Li,* Qian-Ying Li, Qun Guan and Yu-Bin Dong*

College of Chemistry, Chemical Engineering and Materials Science, Collaborative Innovation Center of Functionalized Probes for Chemical Imaging in Universities of Shandong, Key Laboratory of Molecular and Nano Probes, Ministry of Education, Shandong Normal University, Jinan 250014, P. R. China

Email: yananli@sdnu.edu.cn, yubindong@sdnu.edu.cn.

‡ These authors contributed equally.

1. Materials and instrumentation.

All of the starting materials were purchased from commercial sources, unless otherwise noted, and used without further purification. Fourier transform infrared (FTIR) samples were prepared as KBr pellets, and spectra were obtained in the 400-4000 cm^{-1} range using a Perkin-Elmer 1600 FTIR spectrometer. ^{1}H NMR data were collected using an AM-400 spectrometer. Chemical shifts are reported in δ relative to TMS. Fluorescence spectra were obtained with FLS-920 Edinburgh Fluorescence Spectrometer with a Xenon lamp. The scanning electron microscopy (SEM) micrographs were recorded on a Gemini Zeiss Supra TM scanning electron microscope. The X-ray diffraction (XRD) experiments were obtained on a D8 ADVANCE X-ray powder diffractometer with Cu*K*α radiation (λ = 1.5405 Å). The Brunauer-Emmett-Teller (BET) surface area was measured on an ASAP 2020/TriStar 3000 (Micromeritics) using nitrogen adsorption at 77 K. Inductively Coupled Plasma Optical Emission Spectrometer (ICP-OES) measurement was performed on Thermo Scientific iCAP 7400. Confocal fluorescence imaging studies were performed with a TCS SP5 confocal laser scanning microscopy (Leica Co., Ltd. Germany) with an objective lens (×20). The microscope images of crystals were collected on Leica DMI3000B inverted microscope. The crystal data were obtained by Agilent SuperNova X-Ray single crystal diffractometer.

2. Synthesis of H_2L-NH_2.[1]

A mixture of 2,5-dibromoaniline (10 mmol, 2.51 g), 4-methoxyl carbonylphenylboronic acid (30 mmol, 5.4 g), CsF (47.5 mmol, 7.22 g), tetrakis(triphenylphosphine) palladium (1.56 mmol, 1.9 g) and anhydrous dioxane (150 mL) was refluxed for 2 days under nitrogen atmosphere. After cooling to room temperature, the solvent was evaporated to dryness. The residue was washed with water, and purified on column (silica gel, CH2Cl2 : ethylacetate = 40 : 1) to give the esterified ligand as yellow solid (2.5 g, yield: 66%). IR (KBr pellet cm−1): 3458 (m), 3367 (m), 2945 (m), 1703 (s), 1603 (s), 1433 (s), 1283 (m), 1120 (w), 766 (s), 703 (s). 1HNMR(300 MHz, DMSO-d6, 25°C, TMS, ppm): 8.05-8.02 (d, 4H, -C6H4-), 7.78-7.75 (d, 2H, -C6H4-), 7.64-7.62 (d, 2H, -C6H4-), 7.17-7.16 (d, 1H, -C6H3-), 7.15 (s, 1H, -C6H3-), 7.03-7.00 (d, 1H, -C6H3-), 5.10 (s, 2H, -NH2), 3.88 (s, 6H, -CH3). Elemental analysis (%) calcd for C22H19NO4: C 73.12, H 5.30, N 3.88; Found: C 73.54, H 5.70, N 3.36.

The esterified ligand (1.66 mmol, 0.60 g) was stirred in THF (20 mL), to which an aqueous solution of KOH (3.0 g, 53.6 mmol) (50 mL) was added. This mixture was heated at 50°C for 12 h. After removal of THF in vacuum, water was added inside. The mixture was heated until the solid was fully dissolved, then the solution was acidified with diluted HCl until no precipitate formed (pH<2). The green yellow powder was collected by filtration, washed with water and dried in air (0.45 g, yield: 81.4%). IR (KBr pellet cm−1): 2887 (s), 1683 (s), 1603 (m), 1518 (s), 1387 (m), 1287 (m), 1235 (s), 1181 (m), 1112 (w), 769 (s). 1HNMR (300 MHz, DMSO-d6, 25°C, TMS, ppm): 8.05-8.03 (d, 4H, -C6H4-), 7.78-7.75 (d, 2H, -C6H4-), 7.66-7.64 (d, 2H, -C6H4-), 7.44-7.42 (d, 1H, -C6H3-), 7.35 (s, 1H, -C6H3-), 7.33-7.30 (d, 1H, -C6H3-), 4.47 (s, 2H, -NH2). Elemental analysis (%) for

$C_{20}H_{15}NO_4$: C 72.06, H 4.54, N 4.20; Found: C 71.75, H 4.67, N 4.36.

3. UV-vis spectra of UiO-68-NH_2, UiO-68-NCS, UiO-68-R6G and UiO-68-R6G’.

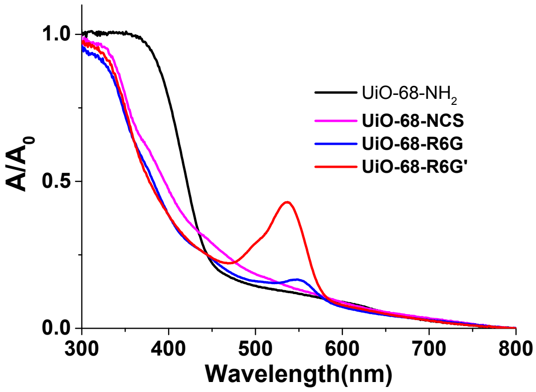

Fig. S1 UV-vis spectra of UiO-68-NH_2, **UiO-68-NCS, UiO-68-R6G and UiO-68-R6G’**.

4. Packing diagram derived from the crystal structures of UiO-68-NH_2 and UiO-68-NCS.

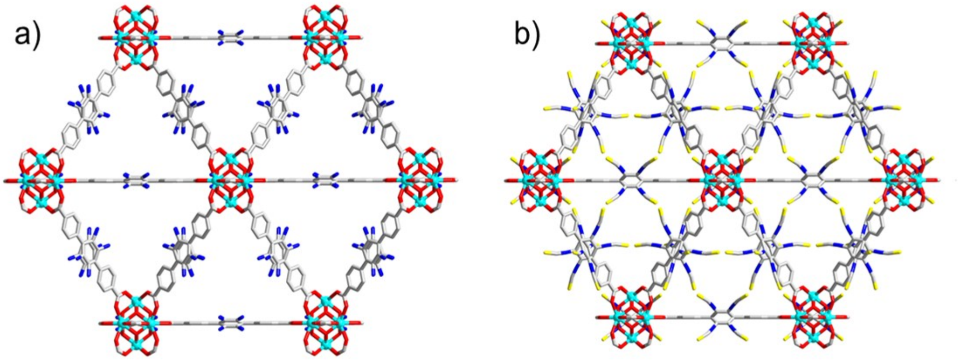

Fig. S2 Packing diagram derived from the crystal structures of UiO-68-NH_2 and **UiO-68-NCS**. Due to the high symmetry of the UiO-68, the positions of the -NH_2 group in UiO-68-NH_2 and the -NCS group in **UiO-68-NCS** were statistically disordered, the occupancy of each group is 12.5%.

5. Functional group transformation based on esterified Me_2L-NH_2.

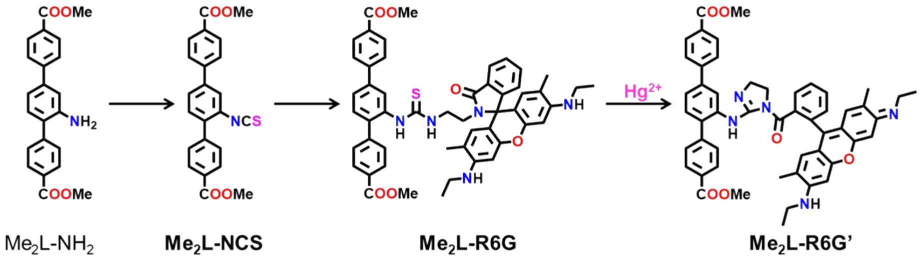

Scheme S1 Synthesis of esterified ligand of **Me_2L-NCS**, **Me_2L-R6G** and **Me_2L-R6G**’.

The esterified ligand of Me_2L-NH_2 (3.6 g, 10 mmol) and triethylamine (0.2 mL, 1.4 mmol) were combined in fresh distilled methylene chloride (20 mL), and then a methylene chloride (5 mL) solution of thiophosgen (1.72

g, 15 mmol) was added dropwise. The obtained mixture was stirred for 12 h at room temperature, then, 2 mL of water added. The organic phase was collected by a separation funnel. After removal of the solvent under reduced pressure, the crude was purified by column on silica gel (methylene chloride) to afford the esterified **Me_2L-NCS** as pale-yellow crystalline solids (4.0 g, yield: 98%). IR (KBr pellet cm^{-1}): 2951 (m), 2175 (m), 2121 (s), 1717 (s), 1707(s), 1608(s), 1431 (s), 1278 (s), 1115 (s), 1018 (m), 825 (m), 770 (s), 706 (w), 484 (w). ^{1}HNMR (400 MHz, DMSO-*d*$_6$, 25°C, TMS, ppm): 8.12 (s, 1H, -C_6H_4-), 8.08-8.04 (d, 4H, -C_6H_4-), 7.98-7.96 (d, 2H, - C_6H_4-), 7.90-7.88 (d, 1H, -C_6H_4-), 7.75-7.73 (d, 2H, -C_6H_3-), 7.67-7.65 (d, 1H, -C_6H_3-), 3.91-3.83 (d, 6H, -CH_3). Elemental analysis (%) calcd for $C_{23}H_{17}NO_4S$: C 68.47, H 4.25, N 3.47, S 7.95; Found: C 68.77, H 4.65, N 3.36, S 7.88.

A mixture of esterified **Me_2L-NCS** (403 mg, 1.0 mmol), *N*-(rhodamine-6G)lactam-ethylenediamine (684 mg, 1.5 mmol) and fresh distilled acetonitrile (40 mL) were refluxed for 24 h under nitrogen atmosphere and stirred for another 2 h at room temperature to form a lot of white precipitate. The solid was filtrated, washed with acetonitrile three times. Crude product was purified by recrystallization from acetonitrile to give esterified **Me_2L-R6G** (720 mg, yield: 84%). IR (KBr pellet cm^{-1}): 3367 (m), 2925 (m), 1711 (s), 1673 (s), 1623 (m), 1520 (m), 1434 (w), 1382 (m), 1281 (s), 1215 (m), 868 (w), 766 (w). ^{1}HNMR (400 MHz, DMSO-*d*$_6$, 25°C, TMS, ppm): 9.15 (s, 1H, -C_6H_3-), 8.07-8.05 (d, 2H, -C_6H_4-), 7.97-7.95 (d, 2H, -C_6H_4-), 7.87-7.85 (d, 2H, -C_6H_4-), 7.77-7.75 (d, 2H, -C_6H_4-), 7.75-7.73 (d, 1H, -C_6H_4-), 7.55-7.54 (d, 2H, -C_6H_4-), 7.54-7.52 (t, 1H, -C_6H_4-), 7.49-7.47 (d, 2H, -C_6H_4-), 7.47-7.44 (t, 1H, -C_6H_4-), 6.94-6.92 (d, 1H, -C_6H_4-), 6.24 (s, 2H, -C_6H_2-), 6.06 (s, 2H, -C_6H_2-), 5.07 (s, 2H, -NH), 3.89 (s, 3H, -CH_3), 3.87 (s, 3H, -CH_3), 3.12-3.08 (t, 8H, -CH_2-), 1.82 (s, 6H, -CH_3), 1.20-1.16 (t, 6H, -CH_3). Elemental analysis (%) calcd for $C_{51}H_{49}N_5O_6S$: C 71.22, H 5.74, N 8.14, S 3.73; Found: C 71.67, H 5.23, N 8.46, S 3.98.

Esterified **Me_2L-R6G** (200 mg, 0.2 mmol) and $Hg(NO_3)_2$ (200 mg, 0.5 mmol) were combined in 100 mL of hot ethanol. The reaction mixture was stayed for 2 h. The solvent was removed and washed with water (3 times). The color of the compound changed to red to generate esterified **Me_2L-6G'**. HRMS (MALDI-TOF) m/z:$[M + H]^+$ calcd for $C_{51}H_{47}N_5O_6$, 826.3599; found, 826.3786.

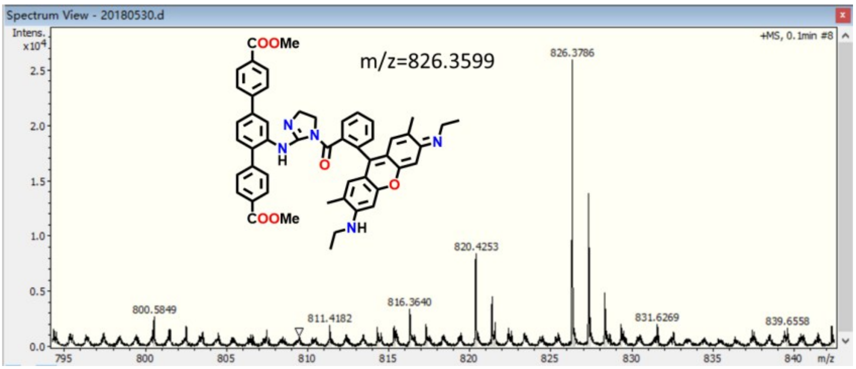

Fig. S3 MS spectra of the esterified **Me_2L-R6G'**.

6. XPS spectra of UiO-68-R6G and UiO-68-R6G’

As show in Fig. S4a, the XPS spectrum of Zr 3d in **UiO-68-R6G** showed two peaks at 185.25 and 182.75 eV, which corresponded to Zr $3d_{3/2}$ and Zr $3d_{5/2}$, respectively. This observation was very similar to that of **UiO-68-R6G'** (185.20 eV and 182.75 eV, Fig. S4b). However, the XPS spectrum of Hg 4f displayed two peaks (101.6 eV, 105.55 eV) in the narrowed bind energy scope (Fig. S4c), which was well in agreement with the reported HgS XPS spectrum.[2] In addition, the peak of S 2p at 162.5 eV was also similar to the reported result for HgS (163.1 eV, Fig. S4d).[2] Therefore, we believe that the Hg^{2+} was present in the form of HgS after the reaction.

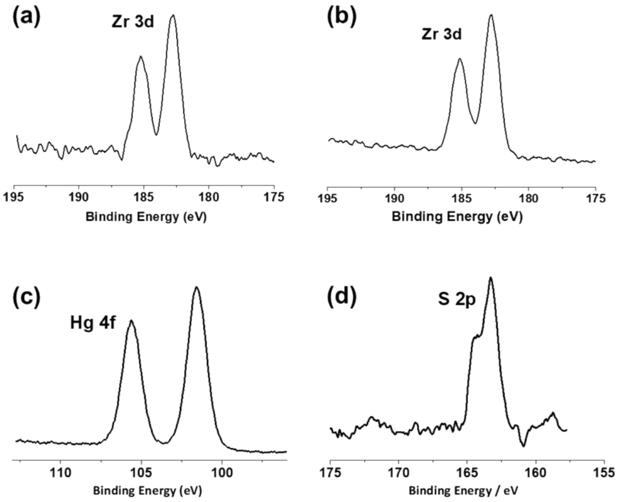

Fig. S4 XPS spectra of **UiO-68-R6G** Zr 3d spectrum (a) and **UiO-68-R6G’** Zr 3d spectrum (b), Hg 4f spectrum (c), S 2p spectrum (d).

7. DLS of the nanosized UiO-68-NH_2, UiO-68-NCS, UiO-68-R6G and UiO-68-R6G’.

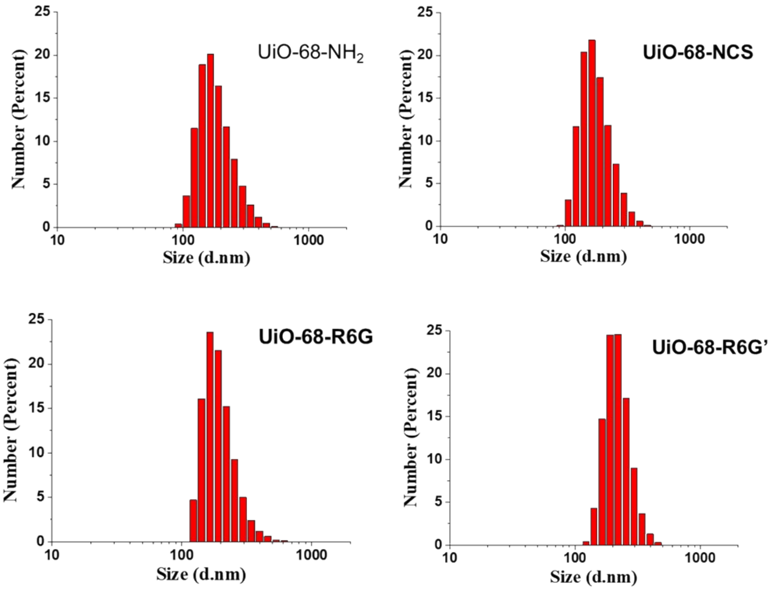

Fig. S5 DLS of the nanosized UiO-68-NH_2, **UiO-68-NCS**, **UiO-68-R6G** and **UiO-68-R6G’**.

8. PXRD of the nanosized UiO-68-NH$_2$, UiO-68-NCS, UiO-68-R6G and UiO-68-R6G’.

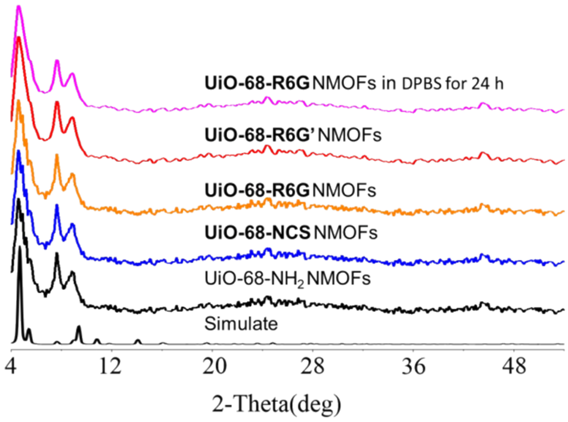

Fig. S6 PXRD patterns of the nanosized UiO-68-NH$_2$, **UiO-68-NCS**, **UiO-68-R6G** and **UiO-68-R6G’**.

9. Fluorescence titration experiment.

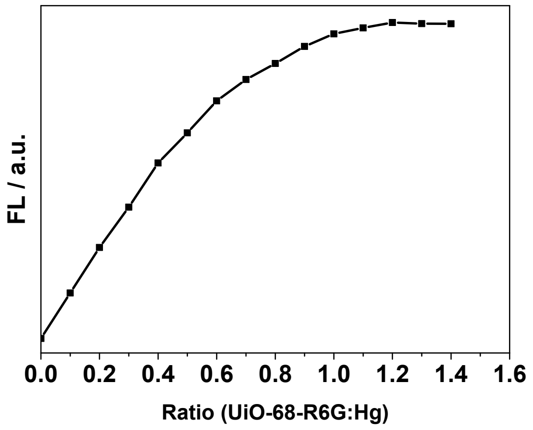

Fig. S7 Fluorescence titration experiment between **UiO-68-R6G** and Hg^{2+} under different ratios.

10. Detection limit and range.

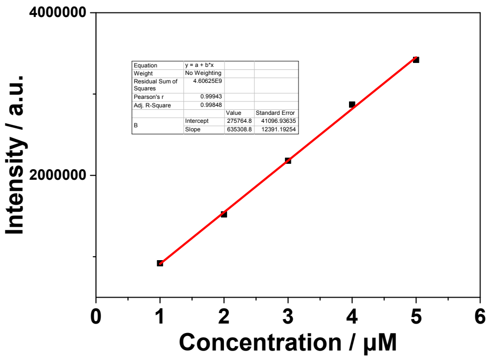

Equation	y = a + b*x		
Weight	No Weighting		
Residual Sum of Squares	4.60625E9		
Pearson's r	0.99943		
Adj. R-Square	0.99848		
		Value	Standard Error
B	Intercept	275764.8	41096.93635
	Slope	635308.8	12391.19254

Fig. S8 Limit of detection (LOD) was determined as 0.10 nM based on LOD = 3 σ/k (where σ = standard deviation and k = slope of the linear plot).

Compared to the reported MOF-based Hg^{2+} probes, **UiO-68-R6G** is one of the most sensitive sensors with the widest detection range for Hg^{2+} under the simulated physiological conditions (Table S1).

Table S1 Summary of the reported MOF-based fluorescent probes for Hg^{2+} under physiological conditions.

Reagent	detection range (μM)	Limit of detection (LOD) (nM)	Refs.
Cd-MOF	0.12-600	ca. 120	3
UiO-66-NH_2 Hybrid System	0.1-10	17.6	4
Zn-MOF	4.98-1055.23	320	5
BSA–AuNPs@Tb–AMP MOFs	0.05-1	20.9	6
TMU-34(-2H)	-	1800	7
Eu^{3+}/CDs@MOF-253	0.065-150	13	8
P-DNA@MOF	-	3.2	9
Pb-MOF	40-160	2149	10
UiO-68-R6G	$0.01\text{-}10^5$	0.10	**This work**

11. MTT assay.

Cells were transferred to a 48-well plate with a cell number of ~10k cells/well and incubated overnight. After removal of the culture medium, the cells were incubated with **UiO-68-R6G** dispersion (200 μL, concentration gradient 0−50 μg/mL) for 1 h. The dispersion was removed, and every well was washed once with DPBS (200 μL). After removal of DPBS, culture medium (200 μL) was added to each well. After incubation for 24 h, MTT (3-(4,5-dimethyl-2-thiazolyl)-2,5-diphenyl-2*H*-tetrazolium bromide, 20 μL, 5 mg/mL) was added and left for 4 h. The supernatant was removed by centrifugation. The precipitate was dissolved in dimethyl sulfoxide (DMSO; 200 μL), and the absorbance at 490 nm was measured.

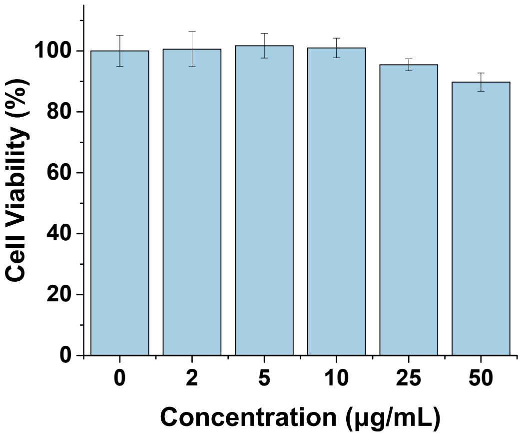

Fig. S9 MTT assay of Hela cells in the presence of different concentrations of **UiO-68-R6G**.

12. X-ray Structural Determination and Single crystal data.

X-ray intensity data were measured at 100 K on an Agilent SuperNova CCD-based diffractometer (Cu Kα radiation, λ = 1.54184 Å). After determination of crystal quality and initial tetragonal unit cell parameters, a hemi sphere of frame data was collected. The raw data frames were integrated with CrysAlisPro, Agilent Technologies, Version 1.171.36.32 (release 02-08-2013 CrysAlis171. NET) (compiled Aug 2 2013, 16 : 46 : 58). Empirical absorption correction using spherical harmonics, implemented in SCALE3 ABSPACK scaling algorithm. Analysis of the data showed negligible crystal decay during data collection. The structure was solved by a combination of direct methods and difference Fourier syntheses, and refined by full-matrix least-squares against F^2, using the SHELXTL software package. A large void space is present in the framework, which contains many significant electron density peaks. The species in this region were too severely disordered to be modeled, and were treated with SQUEEZE/PLATON. The functional groups at the central benzene ring are statistically disordered and subject to large thermal vibration and disorder. They were not resolved in the electron map and have been omitted from the structural model. The sum formula given is for the actual compound including the substituents at the central benzene ring, but ignoring unresolved solvate molecules. Crystal data and structure determination summary for UiO-68-NH_2, **UiO-68-NCS**, **UiO-68-R6G**, **UiO-68-R6G'** are listed in Table S2. CCDC 1847052, 1847053, 1856366 and 1856367 contain the supplementary crystallographic data for this paper. These data can be obtained free of charge from The Cambridge Crystallographic Data Centre via www.ccdc.cam.ac.uk/data_request/cif.

Table S2 Crystal data of UiO-68-NH_2, **UiO-68-NCS**, **UiO-68-R6G** and **UiO-68-R6G'.**

compound	UiO-68-NH_2	**UiO-68-NCS**	**UiO-68-R6G**	**UiO-68-R6G'**
empirical formula	$C_{120}H_{78}N_6O_{32}Zr_6$	$C_{126}H_{66}N_6O_{32}S_6Zr_6$	$C_{120}H_{66}O_{32}Zr_6$	$C_{120}H_{66}O_{32}Zr_6$
formula weight	2663.2	2915.99	2567.04	2567.04
temp (K)	100.0(1)	100.0(1)	150.0(1)	150.0(1)
crystal system	cubic	cubic	cubic	cubic
space group	*Fm-3m*	*Fm-3m*	*Fm-3m*	*Fm-3m*
a (Å)	32.7135(3)	32.6875(2)	32.7408(7)	32.635(4)
b (Å)	32.7135(3)	32.6875(2)	32.7408(7)	32.635(4)
c (Å)	32.7135(3)	32.6875(2)	32.7408(7)	32.635(4)
α (deg)	90.00	90.00	90.00	90.00
β (deg)	90.00	90.00	90.00	90.00
γ(deg)	90.00	90.00	90.00	90.00
V (Å^3)	35009.1(10)	34925.7(6)	35097(2)	34758(13)
Z	4	4	4	4

ρ_{calc} (g/cm^3)	0.505	0.554	0.486	0.491
F(000)	5344.0	5824.0	5128.0	5128
data/restraints/params	1696/146/61	1697/155/78	1662/86/53	1696/86/53
GOF on F^2	1.140	1.571	1.105	1.081
final R indices [I > 2sigma(I)]	R_1 = 0.0776 wR$_2$ = 0.2408	R_1 = 0.0986 wR_2 = 0.3190	R_1 = 0.0651 wR_2 = 0.2043	R_1 = 0.0581 wR_2 = 0.1662

13. References.

(1) Y.-A. Li, S. Yang, Q.-K. Liu, G.-J. Chen, J.-P. Ma and Y.-B. Dong, *Chem. Commun.* 2016, **52**, 6517–6520.

(2) C. Han, W. Wang, F. Xie and T. Zhang, *Sep. Purif. Technol.*, 2017, **177**, 223–232.

(3) L. Yang, X. Li, C. Qin, K.-Z. Shao and Z.-M. Su, *CrystEngComm*, 2016, **18**, 4765–4771.

(4) L.-L. Wu, Z. Wang, S.-N. Zhao, X. Meng, X.-Z. Song, J. Feng, S.-Y. Song and H.-J. Zhang, *Chem. Eur. J.*, 2016, **22**, 477–480.

(5) J. Xiao, J. Liu, X. Gao, G. Ji, D. Wang and Z. Liu, *Sens. Actuators, B*, 2018, **269**, 164–172.

(6) K. Cai, M. Zeng, F. Liu, N. Liu, Z. Huang, Y. Song and L. Wang, *Luminescence*, 2017, **32,** 1277–1282.

(7) S. A. A. Razavi, M. Y. Masoomi and A. Morsali, *Inorg. Chem.*, 2017, **56**, 9646–9652.

(8) X.-Y. Xu and B. Yan, *J. Mater. Chem. C*, 2016, **4**, 1543–1549.

(9) P.-P. Hu, N. Liu, K.-Y. Wu, L.-Y. Zhai, B.-P. Xie, B. Sun, W.-J. Duan, W.-H. Zhang and J.-X. Chen, *Inorg. Chem.*, 2018, **57**, 8382–8389.

(10) A. K. Jana and S. Natarajan, *ChemPlusChem*, 2017, **82**, 1153–1163.